Journal of Geography and Cartography (2023) Volume 6 Issue 2
doi: 10.24294/jgc.v6i2.2164

ORIGINAL RESEARCH ARTICLE

Overview of large scale map production with UAV based photogrammetric technique: A case study in Izmir-Cesme territory of Turkey

Yalçın Yılmaz, Mert Gürtürk, Barış Süleymanoğlu, Arzu Soycan, Metin Soycan*

Department of Geomatic Engineering, Faculty of Civil Engineering, Yildiz Technical University, 34220 Istanbul, Turkey

*** Corresponding author:** Metin Soycan, soycan@yildiz.edu.tr

ABSTRACT

UAVs, also known as unmanned aerial vehicles, have emerged as an efficient and flexible system for offering a rapid and cost-effective solution. In recent years, large-scale mapping using UAV photogrammetry has gained significant popularity and has been widely adopted in academia as well as the private sector. This study aims to investigate the technical aspects of this field, provide insights into the procedural steps involved, and present a case study conducted in Cesme, Izmir. The findings derived from the case study are thoroughly discussed, and the potential applications of UAV photogrammetry in large-scale mapping are examined. The study area is divided into 12 blocks. The flight plans and the distrubition of ground control point (GCP) locations were determined based on these blocks. As a result of the data processing procedure, average GCP positional errors ranging from 1 to 18 cm have been obtained for the blocks.

***Keywords*:** UAV; DEM; DSM; GCP; map production; photogrammetry

ARTICLE INFO

Received: 26 May 2023
Accepted: 21 July 2023
Available online: 9 September 2023

1. Introduction

Large-scale maps exhibit a higher level of detail while encompassing a smaller geographic area. These maps are characterized by a reduced geographic extent when compared to smaller scale maps, resulting in a smaller numerical value positioned to the right of the ratio when expressed as a representative scale. The need of large scale maps with exact and high-resolution topographic mapping data for understanding earth's topography is becoming more widely understood. Topographic mapping serves the purpose of identifying both natural and man-made elements on the earth's surface. Additionally, it visually represents the variations in elevation within the area of interest[1,2]. When unmanned aerial vehicles (UAVs) are used for digital purposes, important points such as digital surface model (DSM) and digital elevation model (DEM) mapping emerge. DSM is a digital map that contains height information of all objects above the earth's surface. DSM maps are used in urban planning, construction projects, forest management, flood analysis, and many other applications. By providing height information of any object above the surface, DSM maps facilitate the analysis of the locations and dimensions of these objects. DEM mapping, on the other hand, provides a model that includes only surface elevation information of the earth. This reflects the earth's hilltops, valleys, slopes, and other topographic features. Digital elevation models, along with X-Y

coordinates on topographic maps, are being increasingly employed in various fields. These models, depicting elevation data, find extensive use among engineers, architects, agronomists, and professionals across diverse disciplines. Technological advancements have facilitated the collection of faster, more precise, and highly accurate data, thereby contributing to the widespread adoption of topographic maps[3]. Within this framework, the production of topographic maps involves the utilization of photogrammetry, remote sensing, LiDAR, and/or traditional surveying techniques such as GPS and Total Station[4,5]. Nonetheless, employing these methods often presents challenges related to operational expertise, software requirements, and occasionally cost[6]. Consequently, there exists a demand for a novel approach that offers comparable accuracy to the aforementioned methods while being economically advantageous.

Unmanned aerial vehicles (UAVs), commonly referred to as drones, are emerging as a viable alternative due to their cost-effectiveness and ability to perform semi- or fully autonomous missions for remote operation and data collection[7]. Compared to other remote sensing platforms, UAVs traditionally provide higher flexibility and speed in image acquisition and data acquisition, and lower cost measurement. Through the utilization of such systems, it becomes possible to obtain detailed and high-resolution images, facilitating the identification and extraction of objects within the imagery[8]. The features mentioned above have led to an increasing utilization of UAVs in various applications, with their usage becoming more prevalent in today's context[9]. However, using UAVs for mapping also presents some challenges. Factors such as determining appropriate viewing angles and flight altitudes, image quality, weather conditions, and the influence of surface coverage must be considered.

The high-resolution images acquired through these systems serve as the foundation for generating topographic maps. The structure from motion (SFM) algorithm utilizes to generate three-dimensional models by aligning and combining overlapping images[10]. This technique enables the creation of high-resolution orthomosaic and digital elevation models using various camera types. The advancements in computer vision and vision analysis have significantly contributed to the successful implementation of SFM in this process[11,12].

The utilization of UAV capabilities has gained significant traction in various map-based applications, experiencing a surge in popularity in recent years[13]. Presently, UAVs are extensively employed across diverse domains, including agriculture, coastal mapping, archaeological survey[14], mining, 3D city modeling, and cadastre applications, reflecting their efficacy and expanding range of applications[15,16]. Regarding to archaeological studies, Manajitprasert et al.[17] utilized drone-captured images and the structure from motion (SfM) technique to generate a three-dimensional (3D) model of the pagodas in wat Maha that. Additionally, the same area underwent scanning with a terrestrial laser scanner. Through a comparative analysis of the models obtained from these two methods using checkpoint analysis, it was observed that both approaches achieved a horizontal accuracy of 6.9 RMSE (root mean square error). The accuracy achieved through the use of unmanned aerial vehicles (UAVs) was deemed satisfactory for archaeological studies.

For urban planning, Elkhrachy[18] studied the accuracy assesment of UAV photogramety. In that study, the accurate geospatial 3D data was generated from UAV images of a 0.05 km^2 area of the Najran university campus in Saudi Arabia using DJI Mavic pro platinum drone. The horizontal and vertical accuracies of the obtained UAV solution were computed by comparing the coordinates of 21 ground control points (GCPs) with coordinates measured using the RTK GPS method. The horizontal RMSE values were 4–6 cm and vertical accuracy was 5–6 cm. The author suggested that utilizing drones along with seven ground control points (GCPs) enables the acquisition of 3D point cloud data for infrastructure projects at a scale of 1:200 with a contour interval of 30 cm. Another study was conducted by Erenoglu et.al.[19]. They used low cost UAV based photogrametry to derive a high spatial resolution DSM and orthophoto mosaic and compared the 3D model derived by UAV with the ones from CORS surveys. The results showed that the accuracy of the UAV photogrammetry was similar to terrestrial surveys commonly used for development plans and city maps.

Additionally, there is a growing trend in incorporating UAV systems for topographic map production, alongside the increasing use of the structure from motion (SfM) algorithm for generating digital elevation models and digital surface model. In the study conducted by Jiménez-Jiménez et al.[20], low cost UAV was preferred for high resolution DSM generation. When the results are analyzed, the authors state that the accuracy of DTMs depends on the UAV system, flight planning and image acquisition, photogrammetric DTM production, and geomorphology and land use/land cover.

The aim of this study is to summarize and explain the general results of the UAV-supported mapping approach, and particularly its potential and contribution to DSM/DEM mapping in test area. The summary and results of this process are important for understanding the rapidly evolving technology of UAVs and their potential in the field of mapping.

2. Flight planning

2.1. Importance of planning the flight path to capture the entire area of interest

There are several criteria to be considered during the planning phase of UAV mapping studies. Firstly, it should be determined whether the flight will be conducted through GNSS-supported autonomous control or manually controlled by the user. In either case, the study area needs to be analyzed beforehand. The study area should be examined for obstacles such as power lines, large trees, sensitive areas, or other potential hazards, and on-site verification should be conducted if necessary. The flight route planning should be performed using available satellite imagery. UAVs can be utilized for real-time event monitoring, change tracking, generating maps or 3D models. Manual control is more suitable for real-time operations, while autonomous control is more favorable for systematic flying required to create a map.

Current UAVs lack advanced detection and collision prevention capabilities and generally fly along pre-determined routes. There can be erroneous behavior of UAVs due to GNSS-related issues, adverse weather conditions, or other technical errors. Therefore, the ability for the user to switch to manual control in case of issues with the autonomous control system is important. Manual control is particularly useful in complex and unpredictable areas such as dense urban regions or forested areas. Even though the planning may be focused on autonomous flights, it is crucial for the user to possess the competence to fly the UAV skillfully in emergency situations.

2.2. Overview of flight planning software for UAVs

Flight route design is an integral part of the UAV mapping process and is commonly carried out using software packages. Open-source software such as mission planner[21] as well as commercial software are frequently utilized. A flight route is defined along parallel lines called “transects” for mapping purposes. This method ensures the collection of a sufficient number of overlapping images.

For optimal results, it is recommended to fly with two overlapping patterns at different altitudes within the same area. This allows for gathering more data and addressing issues related to changes in elevation. However, in some cases, maintaining a constant altitude for the drone is advised[22,23].

Flight plans can be created by users through a flight control device connected to a computer or tablet. Users design the flight route by selecting the camera model, flight altitude, photographing parameters, and other important information. Flight plans are created prior to the flight and then loaded onto the flight control device. When designing flight routes using these methods, the planning process can be facilitated by conducting experiments and tests. This allows for the creation of high-quality and accurate maps.

3. Image capture

The determination of the route is as important as the selection of the captured images along the designated route. In this context, using a digital camera with high resolution, photographs can be taken at the highest possible resolution. The most suitable choice is lenses with a focal length of 50 mm (35 mm film equivalent). It is recommended to use focal lengths between 20 and 80 mm. Wide-angle and fisheye lenses should be avoided, or if used, their distortion should be calibrated to be compatible with the camera model used. While Brown's distortion model[24] is generally sufficient for frame cameras, fisheye and wide-angle lenses are not well represented by this model, so camera calibration with an appropriate distortion model should be performed to process such data.

Fixed lenses should be preferred whenever possible, and if zoom lenses are used, the focal length should be set to the maximum or minimum value throughout the shooting duration to obtain consistent results, and separate camera calibration groups should be defined for different focal lengths.

In UAV-supported mapping studies, image resolution is important. One of the factors that affects this is the ISO value. The ISO value should be set to the lowest level; otherwise, high ISO values can introduce additional noise in the images. The aperture value should be sufficiently high to provide adequate depth of field; capturing sharp and clear photographs is important. The shutter speed should not be too slow, as it can result in blurriness due to slight movements. JPEG compression can introduce unwanted noise in the images; therefore, it is preferable to use RAW data converted to TIFF files for lossless processing.

The scene being captured is another crucial factor in image acquisition. It is challenging to capture images of non-textured, glossy, reflective, or transparent objects. If it is unavoidable to capture such objects, considering shooting in cloudy weather can be helpful. Direct sunlight can create spots on objects and moving lights during the capture can pose difficulties for image processing algorithms. When planning your shots, it is important to avoid unwanted foregrounds, backgrounds, and moving objects. Stay away from flat objects and scenes. The focused subject should be placed to occupy most of the frame. Consider using portrait mode when necessary.

"Snake" and "spiral" routes are the most suitable camera routes. It is noted that capturing images in calm weather and bright light conditions will increase the visible distance. When scanning objects at close range, it is important to take enough photos to minimize the number of "blind spots." Each photo frame should be effectively utilized, and the object of interest should occupy the maximum area.

For aerial photography, the recommended sidelap is 60% and the forward overlap is 80%. In a forested area, it is advised to increase the overlap value to 80% to 90%[25]. Better overlap can be achieved by using cross-flight paths. Using the correct elevation model is crucial for proper flight planning. In low altitudes (less than 300 meters), finding common points may be challenging due to the movement of tree leaves caused by wind. Similarly, caution should be exercised in mountainous areas below 100 meters from the ground. Mapping the same area from the air throughout the entire day is not recommended due to changing lighting conditions. Using photos with different lighting can result in the inability to find common points.

Determining ground control points (GCPs)

Georeferencing is another crucial aspect in the image acquisition process. It involves spatially aligning the UAV-generated map to its real-world location. Georeferencing relies on establishing identifiable points within the images, known as ground control points (GCPs). Homogeneous distribution of GCPs is important to achieve high-quality results through georeferencing. These points can be established using GNSS technologies or traditional ground-based measurements (such as total station). With the advent of drones equipped with real-time positioning units, data can now be obtained with centimeter-level accuracy, reducing

the dependency on GCPs. In areas with significant changes in elevation, fewer GCPs are required compared to drones without positioning information, as this minimizes errors in the vertical component.

4. Image processing

During the image evaluation process, it is important to work with the original images. Manipulations such as cropping or geometric transformations can lead to erroneous results in the processing stage. Such alterations can compromise the integrity of the original content and affect the reliability of the outcomes. Therefore, it is crucial for researchers to preserve the integrity of the original images and perform evaluation processes without any intervention.

Additionally, resizing, or subjecting images to geometric changes is not recommended. Such operations can alter the characteristics of the images and have a negative impact on the results. Resizing, in particular, can lead to pixel loss or degradation, which can affect the authenticity and accuracy of the images. Similarly, geometric changes can distort the perspective or proportions of the images, resulting in incorrect outcomes.

Photometric changes, such as adjustments in brightness or contrast, generally do not significantly affect reconstruction results when applied appropriately. However, it is important to avoid applying harsh filters that can remove fine details (e.g., Gaussian blur filter[26]). Such filters can distort the original structure of the images and lead to incorrect outcomes. Therefore, photometric changes should be applied carefully without compromising the integrity of the images.

In some cases, creating an accurate 3D model from a set of images can be challenging or even impossible. This can be due to unsuitable photographs, such as missing perspective, distorted geometry, or low-quality images, which can hinder the creation of an accurate 3D model. Another factor could be the absence of EXIF data, which provides important parameters for the accurate calibration of the camera, such as sensor pixel size and initial values for focal length. Reliable EXIF data is crucial for obtaining accurate reconstruction results. However, a 3D scene can still be reconstructed without EXIF data. In such cases, the photographs are aligned with a default reasonable focal length value. If the actual focal length significantly deviates from the default value, the alignment process may produce incorrect or even fail to produce satisfactory results.

The first step in image processing is the detection and matching of corresponding points in the photographs, followed by their alignment. This step involves aerial triangulation and bundle adjustment[27]. In this process, camera calibration parameters and camera positions are determined for each image. After this step, a sparse point cloud is generated using the camera parameters and positions.

The next step is to generate a dense point cloud, which requires the optimized sparse point cloud and camera positions. In this optimization process, marked ground control points that are known in coordinates are used. The camera parameters and sparse point cloud are optimized by processing the ground control points in each image. Using the dense point cloud, a three-dimensional “mesh” is created, representing the surface of the object. This mesh provides depth and a sense of volume to the generated data.

In the final step, the original photographs are associated with this data to create textures. This texture helps the data to have a realistic and detailed appearance.

Image processing software

The selection of software packages used for creating maps from UAV-captured images on high-capacity computers is dependent on various factors. These factors include budget, processing power, and the nature of the work to be conducted. As UAV mapping has gained popularity, the market has evolved, leading to a diversity of software packages available for processing. As demand for UAV mapping and photogrammetry software has increased, these programs are regularly updated and improved. In this context, notable software

packages include Autodesk ReCap, Meshroom, 3DF Zephyr, Regard3D, PhotoModeler, Pix4D, Agisoft Photoscan, Colmap, WebODM, and Reality Capture[28].

Pix4D[29] and Agisoft Photoscan[30] are among the most popular data processing options for professional mapping applications. These software packages offer relatively simple user interfaces and understandable guides. However, open-source software options are also available. Software such as Map Knitter, Open Drone Map[31], and structure from motion (VisualSFM)[32] fall into other options. These open-source software packages may have a steeper learning curve but possess strong algorithmic and data processing capabilities despite offering fewer features compared to their paid counterparts.

On the other hand, software like Microsoft ICE[33] may be preferred for panoramic image stitching rather than generating geometrically corrected orthophotos. It should be noted that the lack of standards regarding the proper use and selection of cameras, UAV platforms, and processing software is important to consider when using open-source mapping software and related techniques.

In conclusion, while paid software packages generally offer more user-friendly interfaces and comprehensive features, open-source software packages can provide powerful data processing capabilities despite being free. When making a choice, budget, processing power, and project requirements should be taken into consideration.

5. Test study

The study area is located in the Çeşme region of İzmir province of Turkey and covers an area of 36 km^2 with the dimensions of approximately 8.8 km × 4.4 km as seen in **Figure 1**. The study area is covered by roads, rivers and agricultural fields. As part of a project designed to produce the photogrammetric digital map, images and GNSS data collected from two photogrammetric flights carried out on 20 December 2020 and 06 January 2021 in February (Day of the Year, DoY: 357–006) were used. Fixed-wing SenseFly UAV (unmanned aerial vehicle) was used in the flight. The SenseFly eBee is equipped with L1/L2 GNSS receiver, which realizes RTK solution. In flight, SenseFly S.O.D.A. with a 2.4 × 2.4 μm pixel size with 5472 × 3648 resolution camera is used. A total of 11,701 photos were taken with the UAV. Obtained images were processed with agisoft metashape professional 1.6.2 software, GNSS data PPK (post-process-kinematic) method and SenseFly e motion software. Detailed technical information of the UAV is given in **Table 1**.

Table 1. SenseFly eBee plus UAV and S.O.D.A. camera basic technical specifications[34].

Specialty	Value
Weight/size	1100 g/1100 mm
Cruising speed	40–110 m/s
Max of flight time	About 50 min
PPK/RTK	+
Radiolink distance	3 km
Satellite positioning systems	+
Sensor type/sensor size	RGB (20 mp)/1-inch
Resolution/focal length	5472 × 3648/10.6 mm

According to the flight plan, 6 blocks were defined, 170 m flight altitude, 4 cm/pixel ground resolution and 75% transverse and longitudinal overlaps were predicted. In line with this information, flight routes were calculated for each block, such as block coverage, number of photographs, approximate flight time and flight length, length between consecutive photographs, area covered by one photograph, and shown in Appendix (**Figure A1**).

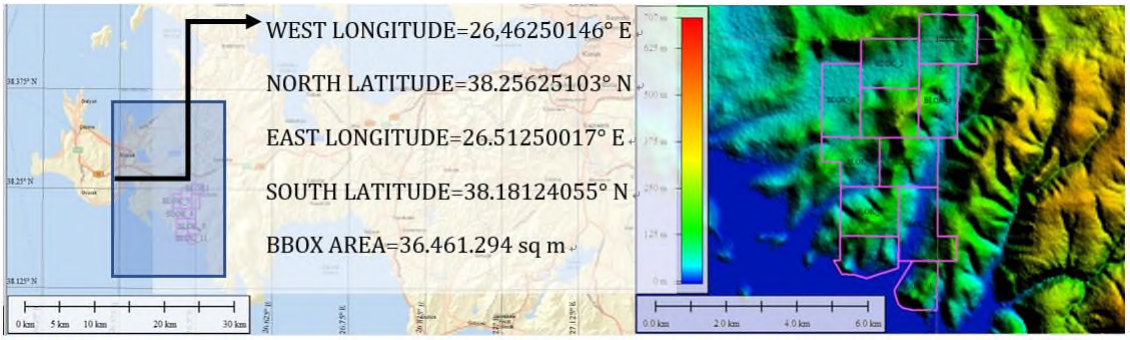

Figure 1. Project site, topographic structure and block designs.

Properly distributed within the blocks, sufficient number and frequency of GCPs were established (**Figure 2**), marked on the field and measured and positioned in the datum and coordinate system where the maps will be produced. Block properties are given in **Table 2**.

Table 2. Block properties.

No.	<Enclosed-area>	<Perimeter>	<Length>	<Width>
Blok-1	2,277,254 m^2	6.057 km	1.641 km	1.387 km
Blok-2	2,277,582 m^2	6.058 km	1.642 km	1.387 km
Blok-3	2,277,758 m^2	6.351 km	2.081 km	1.094 km
Blok-4	2,277,502 m^2	6.057 km	1.641 km	1.387 km
Blok-5	2,277,585 m^2	6.351 km	2.081 km	1.094 km
Blok-6	1,898,676 m^2	6.059 km	-	-
Blok-7	2,277,131 m^2	6.057 km	1.641 km	1.387 km
Blok-8	2,278,828 m^2	6.059 km	1.643 km	1.387 km
Blok-9	2,658,978 m^2	7.446 km	-	-
Blok-10	1,799,438 m^2	5.524 km	-	-
Blok-11	1,405,261 m^2	4.608 km	-	-
Total enclosed-area: 23,705,994 m^2				
Total length/perimeter: 66.627 km				

Evaluations were made separately for each block, and the number of photos used, flight altitude, ground resolution, coverage area, number of anchor points, projection errors, sparse point clouds and related information, as well as merging and optimization parameters are shown in detail in **Table 1**.

Table 3 shows the average GCP (ground control point) position errors obtained in block adjustments. Here, the coordinate values obtained according to the PPK method are compared with the GCP coordinates in the block and the difference values are presented in the table. The 3D difference values obtained show that they vary in the range of 1–18 cm. It is seen that the highest amount of error is in block 2. It is predicted that this result is due to the land structure.

Table 4 shows the average camera position errors obtained in block adjustments. Here, the camera coordinate values obtained according to the RTK and GCP methods are obtained and their errors are presented. The 3D difference values obtained show that they vary in the range of 16–39 cm. It is seen that the highest amount of error is in block 8.

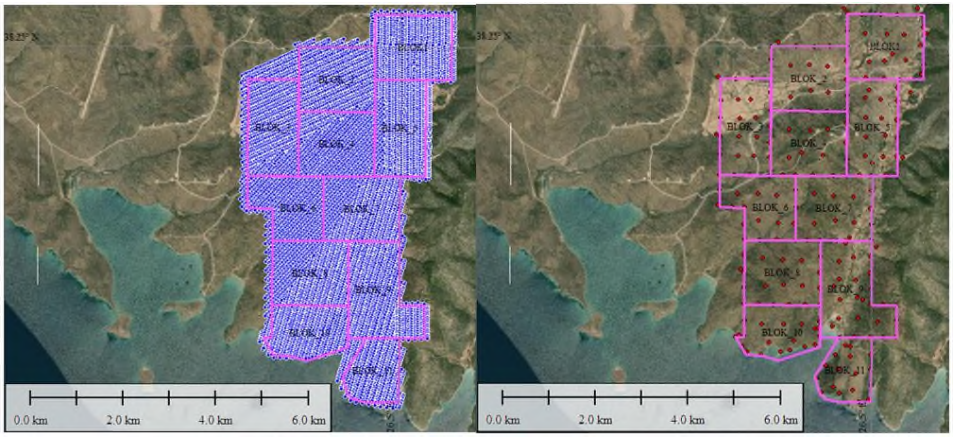

(a) **(b)**

Figure 2. (a) GCP positions blocks; **(b)** camera positions.

Table 3. Average GCP position errors obtained in block balances.

No.	X error (cm)	Y error (cm)	Z error (cm)	XY error (cm)	Total error (cm)
Blok-1	1.82585	2.33017	1.63386	2.96031	3.38126
Blok-2	6.32181	6.25208	15.7722	8.89122	18.1057
Blok-3	1.23547	1.18195	0.997923	1.70979	1.9797
Blok-4	0.71118	1.09722	0.343801	1.30754	1.35199
Blok-5	1.15444	1.52818	0.558648	1.91522	1.99503
Blok-6	0.994862	1.05259	0.589105	1.44835	1.56357
Blok-7	0.982589	1.18138	0.573893	1.5366	1.64027
Blok-8	0.987563	0.843672	0.649687	1.29887	1.45229
Blok-9	0.843701	1.0542	0.854657	1.35025	1.598
Blok-10	0.944297	2.70967	1.08505	2.86949	3.06779
Blok-11-B	0.64687	1.27305	0.380554	1.42797	1.47781
Blok-11-D	5.0621	4.9158	4.59529	7.0562	8.42061

Table 4. Average camera position errors obtained in block adjustments.

No.	X error (cm)	Y error (cm)	Z error (cm)	XY error (cm)	Total error (cm)
Blok-1	4.80974	5.23083	26.3703	7.106	27.3109
Blok-2	9.33323	16.5799	15.1921	19.0264	24.3475
Blok-3	11.7781	11.5136	18.5615	16.4708	24.8156
Blok-4	8.08835	10.7338	10.3237	13.4401	16.9474
Blok-5	13.3803	15.4388	28.7934	20.4301	35.3051
Blok-6	10.6545	10.1748	21.2633	14.7325	25.8684
Blok-7	13.7327	14.5882	28.858	20.0351	35.131
Blok-8	15.2698	20.0529	30.4427	25.2049	39.5227
Blok-9	12.6245	11.2242	21.0126	16.8926	26.9609
Blok-10	2.63676	2.42961	3.10574	3.58546	4.74354
Blok-11-B	8.58858	6.32866	14.3268	10.6684	17.8626
Blok-11-D	5.17554	4.15646	7.10454	6.63795	9.723

Leica Photogrammetry Suite software was used for stereo processing was performed with two simultaneous PC screens as seen in **Figure 3**.

Figure 3. Stereo processing.

On the first PC screen, the model formed by the overlapping regions in the sequentially taken aerial photographs was open (3D raster data), while the work was carried out on the other PC screen using the Microsoft software (2D vector data) working simultaneously with the first screen. The data, which were evaluated as 3D on the first screen, were simultaneously checked as vectors on the second screen, and the work was completed in this way.

In this study, within the scope of photogrammetric base map production in İzmir-Çeşme region, 6 different blocks were defined and according to these blocks, flight plan, aerial photography by UAV, block balancing, point cloud, orthophoto and digital elevation model production and stereo control operations were carried out. Each block has a different number of ground control points. In the study, the results were analyzed in two different types. First, the coordinates calculated by the RTK method were compared with the GCPs. It is seen that the results show a change in the range of 2–8 cm in general and these results show a change independent of the number of GCPs within the block. Secondly, the camera positions were positioned according to the GCPs coordinates and the difference values were calculated. It is seen that these results generally vary in the range of 4–27 cm.

6. Results

In conclusion, this study has effectively demonstrated strict adherence to project requirements regarding flight planning and execution. The aerial photographs were captured at appropriate altitudes with an adequate number, frequency, and resolution. The accuracy of camera positioning was achieved through the utilization of post-measurement kinematic GPS/GNSS processing. Ground control points (GCPs) were precisely established in the TUREF system, with orthometric heights calculated at regular intervals and with exceptional precision. The subsequent data processing steps, including photo stitching, point cloud generation, optimization, and block adjustments, were meticulously carried out using appropriate evaluation software. The results obtained from the block adjustment process aligned remarkably well with the expected standards. The stereo evaluation was performed using a methodologically and theoretically robust approach, ultimately leading to the successful completion of map production Overall, this study serves as a compelling demonstration of the successful implementation of the outlined procedures, effectively achieving the desired outcomes in strict accordance with the project objectives.

The successful implementation of UAV photogrammetry in large-scale mapping requires careful attention to avoid systematic errors originating from processing software, particularly when dealing with precision-demanding scientific applications. The processing of extensive datasets comprising high-resolution images may be time-consuming, necessitating the use of more powerful computer processors for efficient data processing. Advancements in technology will lead to the development of faster processors capable of

processing images at an accelerated rate. Furthermore, improvements in UAV flight endurance, range, and photographic sensor capacities are expected. The increased autonomy levels in both flight software and post-processing software will enable the creation of maps in a faster, more accurate, precise, and cost-effective manner.

The study findings demonstrate the capabilities of drones in capturing high-resolution images and employing image processing and photogrammetry techniques for creating 3D maps and models. Drones serve as effective tools in mapping and navigation applications, enabling the production of accurate maps for large-scale areas such as terrain analysis, construction projects, agriculture monitoring, environmental surveillance, and emergency response. Drones equipped with various sensors and cameras, including thermal cameras, multispectral cameras, and LiDAR, facilitate data collection and analysis. Furthermore, the data collected by these systems can provide a high level of sensitivity and precision. However, it is crucial to remember that the achieved degree of accuracy may vary depending on the quality of the equipment used, flight characteristics, and data processing procedures.

The integration of GPS and other positioning systems facilitates precise navigation and positioning of drones, enabling detailed mapping of targeted areas. However, to ensure the success of large-scale mapping endeavors using drone technology, several critical aspects must be considered. These include data integrity and compatibility, which involve the fusion, calibration, and integration of data from diverse sources, while aligning them with geographic information systems (GIS), as these factors significantly impact various applications. Nonetheless, it is essential to acknowledge that data collection efficiency can be influenced by several factors, such as flight time, battery life, and data storage capacity. Additionally, the cost and duration of large-scale mapping projects are contingent upon factors like the size and complexity of the area being mapped, expenses associated with drones and equipment, the time required for data collection and processing, the expertise of the personnel involved, and the desired resolution and accuracy of the resulting maps.

However, upon examining the accuracy of ground control points (GCPs) in each block, it was observed that certain blocks had lower accuracy compared to others. It is speculated that these discrepancies may be attributed to changes in the topography; however, further investigations are needed to determine the exact reasons. Consequently, future studies are planned to conduct more comprehensive analyses in this regard.

However, it is important to note that the fundamental principles underlying UAV photogrammetry, such as the process of image capture by drones, the integration of multiple images, and their geospatial alignment, are unlikely to undergo significant changes in the foreseeable future. Therefore, while advancements in technology offer enhanced capabilities and efficiency, the core principles of UAV photogrammetry will continue to serve as the foundation for large-scale mapping endeavors. Researchers and practitioners should remain attentive to technological developments while upholding the fundamental principles to ensure the successful application of UAV photogrammetry in future mapping projects.

The UAV-supported mapping approach was observed to yield successful results overall. High levels of resolution and accuracy were achieved, and the data collection and processing procedures were found to be fast and efficient. Additionally, the accuracy and efficiency of automatic feature extraction and classification methods were seen to improve. This has contributed to better decision making in application areas and the improvement of resource management processes. The results demonstrate the significant role of the UAV-supported mapping approach in DSM/DEM mapping, suggesting a potential for use in many sectors. The proposed approach was observed to make significant contributions by providing speed, accuracy, and efficiency in the processes of data collection, processing, and analysis.

Author contributions

Conceptualization, MS and YY; methodology, MS and AS; software, MG; validation, BS, YY and MG; formal analysis, AS; investigation, YY, MG and BS; resources, MS; data curation, YY; writing—original draft preparation, YY, MG and BS; writing—review and editing, YY, MG and BS; visualization, YY; supervision, MS and AS; project administration, AS; funding acquisition, YY. All authors have read and agreed to the published version of the manuscript.

Acknowledgment

The authors would like to thank Anadolu group mapping engineering architecture construction ind. trade. co. ltd. for providing dataset.

This project was undertaken as part of the mapping efforts focusing on Cultural and Tourism Protection and Development Zones(CTPDZ) within the Izmir-Cesme region.

Conflict of interest

The authors declare no conflict of interest.

Reference

1. Ghilani CD, Wolf PR. *Elementary Surveying: An İntroduction to Geomatics*, 13th ed. Pearson College Div; 2012.
2. Wolf PR, Dewitt BA, Wilkinson BE. *Elements of Photogrammetry with Applications in GIS*, 4th ed. McGraw Hill Education; 2014.
3. Kumar NS, Ismail MAM, Sukor NSA, Cheang W. Geohazard reconnaissance mapping for potential rock boulder fall using low altitude UAV photogrammetry. *IOP Conference Series Materials Science and Engineering* 2018; 352(1): 012033. doi: 10. 1088/1757-899X/352/1/012033
4. Lato MJ, Hutchinson DJ, Gauthier D, et al. Comparison of airborne laser scanning, terrestrial laser scanning, and terrestrial photogrammetry for mapping differential slope change in mountainous terrain. *Canadian Geotechnical Journal* 2014; 52(2): 129–140. doi: 10.1139/cgj-2014-0051
5. Tang P, Vick S, Chen J, Paal SG. Chapter 2: Surveying, geomatics, and 3D reconstruction. In: *Infrastructure Computer Vision*. Elsevier; 2020. pp. 13–64.
6. James MR, Ilic S, Ruzic I. Measuring 3D coastal change with a digital camera. In: Proceedings of the Coastal Dynamics 2013; 24–28 June 2013; Bordeaux, France. pp. 893–904.
7. Sanchez‐Azofeifa A, Guzmán JA, Campos CA, et al. Twenty‐first century remote sensing technologies are revolutionizing the study of tropical forests. *Biotropica* 2017; 49(5): 604–619. doi: 10.1111/btp.12454
8. Ndehedehe C. Chapter 8: Remotely piloted aircraft system. In: *Satellite Remote Sensing of Terrestrial Hydrology*. Springer; 2022.
9. Goncalves JA, Henriques R. UAV photogrammetry for topographic monitoring of coastal areas. *ISPRS Journal of Photogrammetry and Remote Sensing* 2015; 104: 101–111. doi: 10. 1016/j.isprs jprs. 2015.02.009
10. Westoby MJ, Brasington J, Glasser NF, et al. Structure-from-motion photogrammetry: A novel, low-cost tool for geomorphological applications. *Geomorphology* 2012; 179: 300–314. doi: 10.1016/j.geomo rph.2012.08.021
11. Javernick L, Brasington J, Caruso B. Modelling the topography of shallow braided rivers using structure-from-motion photogrammetry. *Geomorphology* 2014; 213: 166–182. doi: 10.1016/j.geomorph.2014.01.006
12. Brunier G, Fleury JT, Anthony E, et al. Closerange airborne structure-from-motion photogrammetry for high-resolution beach morphometric surveys: Examples from an embayed rotating beach. *Geomorphology* 2016; 261: 76–88. doi: 10.1016/j.geomo rph.2016.02.025
13. Deliry SI, Avdan U. Accuracy of unmanned aerial systems photogrammetry and structure from motion in surveying and mapping: A review. *Journal of the Indian Society of Remote Sensing* 2021; 49(7): 1997–2017. doi: 10.1007/s12524-021-01366-x
14. Barba S, Barbarella M, Benedetto AD, et al. Quality assessment of UAV photogrammetric archaeological survey. *The International Archives of the Photogrammetry, Remote Sensing and Spatial Information Sciences* 2019; 42: 93–100. doi: 10.5194/isprs-archives-XLII-2-W9-93-2019
15. Pereira P, Baptista P, Cunha T, et al. Estimation of the nearshore bathymetry from high temporal resolution sentinel-1A C-band SAR data—A case study. *Remote Sensing Environment* 2019; 223: 166–178. doi: 10.1016/j.rse.2019.01.003

16. Baloloy AB, Lanco AC, Anaa RRCS, Nadaoka K. Development and application of a new mangrove vegetation index (MVI) for rapid and accurate mangrove mapping. *ISPRS Journal of Photogrammetry and Remote Sensing* 2020; 166(3): 95–117. doi: 10.1016/j.isprsjprs.2020.06.001
17. Manajitprasert S, Tripathi NK, Arunplod S. Three-dimensional (3D) modeling of cultural heritage site using UAV imagery: A case study of the pagodas in wat Maha that, Thailand. *Applied Sciences* 2019; 9(18): 3640. doi: 10.3390/app9183640
18. Elkhrachy I. Accuracy assessment of low-cost unmanned aerial vehicle (UAV) photogrammetry. *Alexandria Engineering Journal* 2021; 60(6): 5579–5590. doi: 10.1016/j.aej.2021.04.011
19. Erenoglu RC, Erenoglu O, Arslan N. Accuracy assessment of low cost UAV based city modelling for urban planning. *Tehnicki Vjesnik* 2018; 25(6): 1708–1714. doi: 10.17559/TV-20170904202055
20. Jiménez-Jiménez SI, Ojeda-Bustamante W, Marcial-Pablo MDJ, Enciso J. Digital terrain models generated with low-cost UAV photogrammetry: Methodology and accuracy. *ISPRS International Journal of Geo-Information* 2021; 10(5): 285. doi: 10.3390/ijgi10050285
21. Mission Planner 2023. Available online: https://ardupilot.org/planner/index.html (accessed on 22 May 2023).
22. He J, Li Y, Zhang K. Research of UAV flight planning parameters. *Positioning* 2012; 3(4): 43–45. doi: 10.4236/pos.2012.34006
23. Nex F, Remondino F. UAV for 3D mapping applications: A review. *Applied Geomatics* 2014; 6(1): 1–15. doi: 10.1007/s12518-013-0120-x
24. Brown DC. Close-range camera calibration. *Photogrammetric Engineering* 1971; 37: 855–866.
25. Elhadary A, Rabah M, Ghanim E, et al. The influence of flight height and overlap on UAV imagery over featureless surfaces and constructing formulas predicting the geometrical accuracy. *NRIAG Journal of Astronomy and Geophysics* 2022; 11(1): 210–223. doi: 10.1080/20909977.2022.2057148
26. Haddad RA, Akansu AN. A class of fast gaussian binomial filters for speech and image processing. *IEEE Transactions on Signal Processing* 1991; 39(3): 723–727. doi: 10.1109/78.80892
27. Triggs B, McLauchlan PF, Hartley RI, Fitzgibbon AW. Bundle adjustment—A modern synthesis. In: Triggs B, Zisserman A, Szeliski R (edıtors). *Vision Algorithms: Theory and Practice*. Springer, Berlin, Heidelberg; 2022. Volume 1883. pp. 298–372.
28. Available online: https://www.3dsourced.com/3d-software/best-photogrammetry-software/ (accessed on 22 May 2023).
29. Available online: https://support.pix4d.com/hc/en-us/articles/204272989-Offline-Getting-Started-and-Manual-pdf (accessed on 21 August 2023).
30. Agisoft photoscan user manual. Available online: https://www.agisoft.com/pdf/photoscan-pro_1_4_en.pdf (accessed on 21 August 2023).
31. Giuseppina VACCA. WEB open drone map (WebODM) a software open source to photogrammetry process. In: Proceedings of the FIG Working Week 2020—CANCELLED—Smart Surveyors for Land and Water Management; 10–14 May 2020; Amsterdam, Netherlands.
32. Morgan JA, Brogan DJ. How to VisualSFM. Available online: https://www.engr.colostate.edu/~jamorgan/How_to_VisualSFM.pdf (accessed on 21 August 2023).
33. Image composite editor. Available online: https://www.microsoft.com/en-us/research/project/image-composite-editor/ (accessed on 22 May 2023).
34. SenseFly. Available online: https://www.paksoyteknik.com.tr/paksoy-topcon/iha/SenseFly-ebee-plus.SenseFly (accessed on 1 May 2023).

Appendix

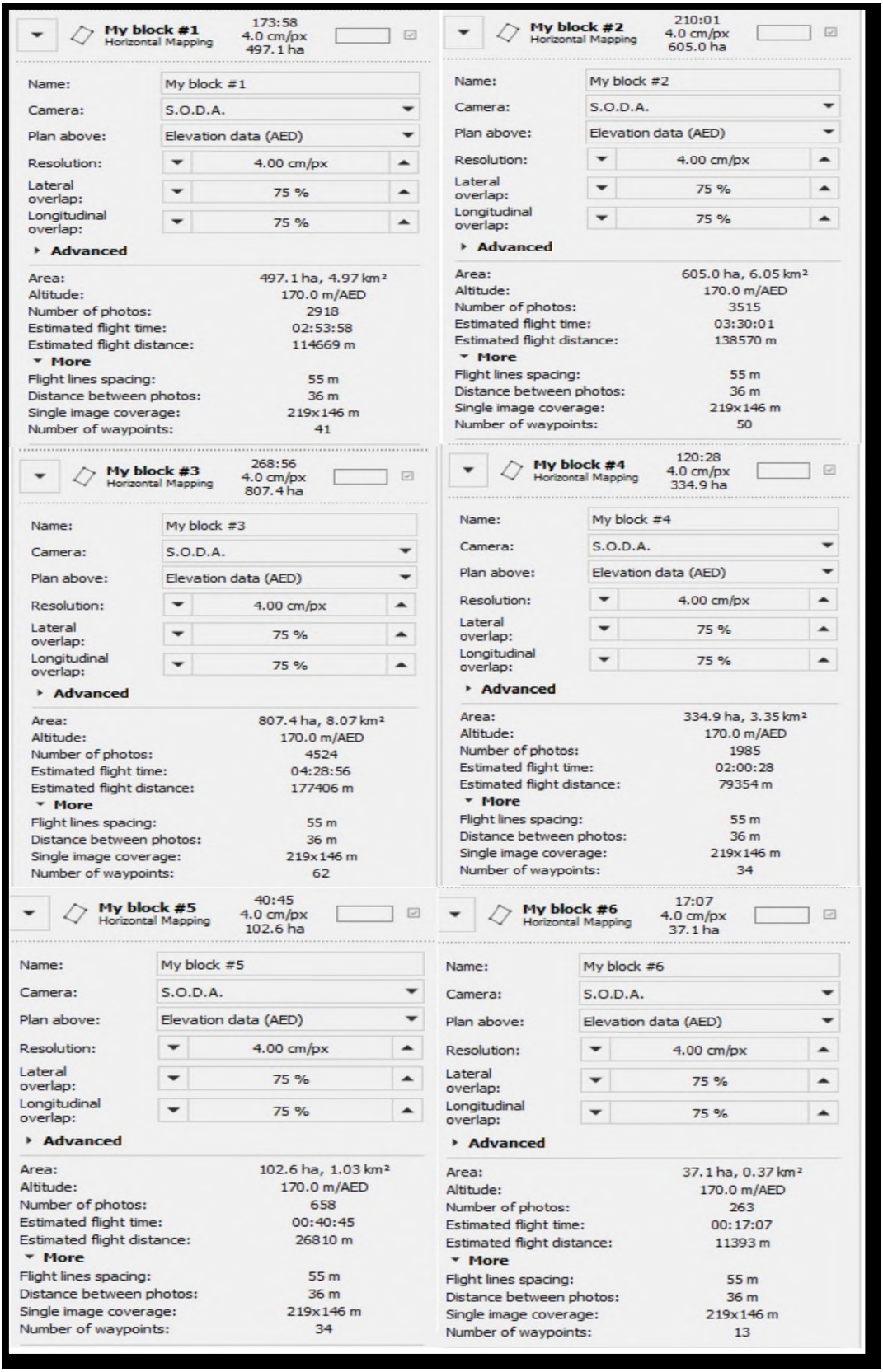

Figure A1. Flight plan and flight blocks design.

Table A1. Summary of evaluation parameters and evaluation results.

Coordinate system TUREF/TM27 (EPSG: 5253) **Rotation angles** Yaw, pitch, roll **Optimization parameters** Parameters f, b1, b2, cx, cy, k1-k4, p1, p2 Adaptive camera model fitting	**Alignment parameters** Accuracy high Generic preselection yes Reference preselection source Key point limit 40,000 Tie point limit 4000 Guided image matching no Adaptive camera model fitting yes

Blok no	**General**	**Point cloud**
1 Number of images: 1310 Flying altitude: 240 m Ground resolution: 5.45 cm/pix Coverage area: 1.93 km^2 Camera stations: 1310 Tie points: 615,052 Projections: 4,857,792 Reprojection error: 1.2 pix	Cameras 1310 Aligned cameras 1310 Markers 32	Points 615,052 of 712,725 RMS reprojection error 0.191051 (1.19501 pix) Max reprojection error 2.51837 (44.3185 pix) Mean key point size 6.05116 pix Point colors 3 bands, uint8 Key points no Average tie point multiplicity 8.79353
2 Number of images: 1765 Flying altitude: 223 m Ground resolution: 5.07 cm/pix Coverage area: 2.46 km^2 Camera stations: 1765 Tie points: 957,528 Projections: 6,017,280 Reprojection error: 0.788 pix	Cameras 1765 Aligned cameras 1765 Markers 39	Points 957,528 of 1,120,707 RMS reprojection error 0.204821 (0.787576 pix) Max reprojection error 1.53023 (38.3821 pix) Mean key point size 3.70825 pix Point colors 3 bands, uint8 Key points no Average tie point multiplicity 7.01206
3 Number of images: 1729 Flying altitude: 239 m Ground resolution: 5.42 cm/pix Coverage area: 2.86 km^2 Camera stations: 1729 Tie points: 710,932 Projections: 5,753,723 Reprojection error: 0.764 pix	Cameras 1729 Aligned cameras 1729 Markers 27	Points 710,932 of 875,768 RMS reprojection error 0.22186 (0.764344 pix) Max reprojection error 2.01841 (29.4971 pix) Mean key point size 3.3999 pix Point colors 3 bands, uint8 Key points no Average tie point multiplicity 8.83089
4 Number of images: 2149 Flying altitude: 234 m Ground resolution: 5.31 cm/pix Coverage area: 2.53 km^2 Camera stations: 2149 Tie points: 1,025,767 Projections: 7,446,596 Reprojection error: 0.75 pix	Cameras 2149 Aligned cameras 2149 Markers 32	Points 1,025,767 of 1,216,425 RMS reprojection error 0.200343 (0.749695 pix) Max reprojection error 1.82901 (29.4555 pix) Mean key point size 3.70822 pix Point colors 3 bands, uint8 Key points no Average tie point multiplicity 7.76169
5 Number of images: 2262 Flying altitude: 235 m Ground resolution: 5.33 cm/pix Coverage area: 3.55 km^2 Camera stations: 2262 Tie points: 1,420,857 Projections: 8,169,711 Reprojection error: 0.878 pix	Cameras 2262 Aligned cameras 2262 Markers 42	Points 1,420,857 of 1,572,680 RMS reprojection error 0.204938 (0.877767 pix) Max reprojection error 1.03996 (33.7761 pix) Mean key point size 3.95666 pix Point colors 3 bands, uint8 Key points no Average tie point multiplicity 6.41403

Table A1. (*Continued*).

Blok no	General	Point cloud
6 Number of images: 2182 Flying altitude: 287 m Ground resolution: 6.52 cm/pix Coverage area: 2.62 km^2 Camera stations: 2182 Tie points: 743,879 Projections: 7,801,989 Reprojection error: 0.728 pix	Cameras 2182 Aligned cameras 2182 Markers 40	Points 743,879 of 883,275 RMS reprojection error 0.216291 (0.728163 pix) Max reprojection error 0.962627 (24.2689 pix) Mean key point size 3.37157 pix Point colors 3 bands, uint8 Key points no Average tie point multiplicity 12.014
7 Number of images: 2064 Flying altitude: 246 m Ground resolution: 5.59 cm/pix Coverage area: 2.52 km^2 Camera stations: 2064 Tie points: 1,335,848 Projections: 7,754,384 Reprojection error: 0.821 pix	Cameras 2064 Aligned cameras 2064 Markers 39	Points 1,335,848 of 1,443,259 RMS reprojection error 0.195094 (0.820874 pix) Max reprojection error 0.953231 (29.7681 pix) Mean key point size 3.9789 pix Point colors 3 bands, uint8 Key points no Average tie point multiplicity 6.35021
8 Number of images: 2326 Flying altitude: 263 m Ground resolution: 5.97 cm/pix Coverage area: 2.67 km^2 Camera stations: 2325 Tie points: 1,091,650 Projections: 8,957,048 Reprojection error: 0.795 pix	General Cameras 2326 Aligned cameras 2325	Points 1,091,650 of 1,218,911 RMS reprojection error 0.213384 (0.794699 pix) Max reprojection error 0.975865 (34.3807 pix) Mean key point size 3.68374 pix Point colors 3 bands, uint8 Key points no Average tie point multiplicity 9.29073
9 Number of images: 1690 Flying altitude: 227 m Ground resolution: 5.15 cm/pix Coverage area: 3 km^2 Camera stations: 1682 Tie points: 1,458,168 Projections: 6,144,788 Reprojection error: 0.84 pix	Cameras 1690 Aligned cameras 1682 Markers 42	Points 1,458,168 of 1,572,210 RMS reprojection error 0.183002 (0.839693 pix) Max reprojection error 0.988211 (34.7628 pix) Mean key point size 4.22656 pix Point colors 3 bands, uint8 Key points no Average tie point multiplicity 4.44671
10 Number of images: 1623 Flying altitude: 258 m Ground resolution: 5.85 cm/pix Coverage area: 2.21 km^2 Camera stations: 1623 Tie points: 789,761 Projections: 5,942,743 Reprojection error: 0.881 pix	Cameras 1623 Aligned cameras 1623 Markers 39	Points 789,761 of 876,613 RMS reprojection error 0.215836 (0.881295 pix) Max reprojection error 0.989472 (40.0242 pix) Mean key point size 3.99018 pix Point colors 3 bands, uint8 Key points no Average tie point multiplicity 8.58565
11 B Number of images: 546 Flying altitude: 232 m Ground resolution: 5.28 cm/pix Coverage area: 0.933 km^2 Camera stations: 523 Tie points: 471,451 Projections: 1,713,599 Reprojection error: 0.775 pix	Cameras 546 Aligned cameras 523 Markers 22	Points 471,451 of 496,893 RMS reprojection error 0.162891 (0.774857 pix) Max reprojection error 0.677038 (34.7088 pix) Mean key point size 4.33696 pix Point colors 3 bands, uint8 Key points no Average tie point multiplicity 3.80167

Table A1. (*Continued*).

Blok no	General	Point cloud
11 D Number of images: 472 Flying altitude: 223 m Ground resolution: 5.06 cm/pix Coverage area: 1.12 km^2 Camera stations: 472 Tie points: 348,988 Projections: 1,877,502 Reprojection error: 0.821 pix	Cameras 472 Aligned cameras 472 Markers 12	Points 348,988 of 373,269 RMS reprojection error 0.194345 (0.821266 pix) Max reprojection error 0.680254 (19.9814 pix) Mean key point size 4.0005 pix Point colors 3 bands, uint8 Key points no Average tie point multiplicity 5.6855